TU Delft

Delft University of Technology

Effect of Al_2O_3 content in slag on the relationship between slag reactivity and carbonation resistance

Zhang, Yu; Çopuroğlu, Oğuzhan

DOI
10.1080/21650373.2023.2250786

Publication date
2023

Document Version
Final published version

Published in
Journal of Sustainable Cement-Based Materials

Citation (APA)
Zhang, Y., & Çopuroğlu, O. (2023). Effect of Al_2O_3 content in slag on the relationship between slag reactivity and carbonation resistance. *Journal of Sustainable Cement-Based Materials*, *13*(1), 33-48. Article 2250786. https://doi.org/10.1080/21650373.2023.2250786

Important note
To cite this publication, please use the final published version (if applicable).
Please check the document version above.

Copyright
Other than for strictly personal use, it is not permitted to download, forward or distribute the text or part of it, without the consent of the author(s) and/or copyright holder(s), unless the work is under an open content license such as Creative Commons.

Takedown policy
Please contact us and provide details if you believe this document breaches copyrights.
We will remove access to the work immediately and investigate your claim.

This work is downloaded from Delft University of Technology.
For technical reasons the number of authors shown on this cover page is limited to a maximum of 10.

Journal of Sustainable Cement-Based Materials

ISSN: (Print) (Online) Journal homepage: https://www.tandfonline.com/loi/tscm20

Effect of Al_2O_3 content in slag on the relationship between slag reactivity and carbonation resistance

Yu Zhang & Oğuzhan Çopuroğlu

To cite this article: Yu Zhang & Oğuzhan Çopuroğlu (2023): Effect of Al_2O_3 content in slag on the relationship between slag reactivity and carbonation resistance, Journal of Sustainable Cement-Based Materials, DOI: 10.1080/21650373.2023.2250786

To link to this article: https://doi.org/10.1080/21650373.2023.2250786

© 2023 The Author(s). Published by Informa UK Limited, trading as Taylor & Francis Group

Published online: 28 Aug 2023.

Submit your article to this journal

Article views: 77

View related articles

View Crossmark data

Full Terms & Conditions of access and use can be found at
https://www.tandfonline.com/action/journalInformation?journalCode=tscm20

Journal of Sustainable Cement-Based Materials, 2023
http://dx.doi.org/10.1080/21650373.2023.2250786

Taylor & Francis
Taylor & Francis Group

OPEN ACCESS Check for updates

Effect of Al_2O_3 content in slag on the relationship between slag reactivity and carbonation resistance

Yu Zhang* and Oğuzhan Çopuroğlu

Microlab, Section Materials and Environment, Faculty of Civil Engineering and Geosciences, Delft University of Technology, Delft, The Netherlands

To understand the influence of slag chemistry on the carbonation resistance of slag-rich cement, this paper explored the carbonation characteristics of blended cement systems with different Al_2O_3 contents in slag through accelerated carbonation test. Irrespective of slag chemistry, three main CO_2 binding phases were identified during accelerated carbonation test, i.e. carbonated Ca-Al AFm phases (amorphous or nano-crystalline), carbonated hydrotalcite-like phase, and calcium carbonate (amorphous calcium carbonate, vaterite, and calcite). Additionally, it was noted that the classification employed for slag reactivity (based on slag chemistry) cannot be extended to predict carbonation resistance of slag-rich cement directly. The main challenge occurred for slag with high alumina content. The experimental results showed that Al_2O_3-rich slag exhibited a high reactivity and can be considered as a reactive component in the blended mixture; however, it did not contribute to carbonation resistance of the mixture. Especially for CO_2 binding capacity, it was similar for systems with varied alumina content in slag (from 3.69 to 18.19 wt.%) in the completely carbonated area.

Keywords: slag-rich cement paste; Al_2O_3; carbonation resistance; slag reactivity; thermodynamic modeling

1. Introduction

Blast furnace slag, which will henceforth be referred to as *slag*, is the by-product of producing pig iron [1]. The iron ore gangue, reduced substances, and components of melted coke are mixed in the furnace to form liquid slag at a temperature of around 1,450 °C [2]. Its major constituents, calcium oxide and silica, are present in large quantities. Also, slag contains significant amounts of minor components, i.e. alumina and magnesium oxide. Therefore, it is commonly expressed as a $CaO-SiO_2-Al_2O_3-MgO$ system. In addition, slag absorbs other accompanying alkalis like Na and K as well as sulfur compounds (trace constituents) [2]. Through rapid cooling with water in ponds, or with powerful water jets, molten slag solidifies immediately and turns into a granular, almost fully non-crystalline, glassy form known as granulated slag. Thus, it is mostly used as a kind of supplementary cementitious material (SCM) in cement industry [3].

Since blast furnace used to be found in the vicinity of iron ore and/or coal deposits, and slag chemistry is strongly related to the compositions of raw materials which can be expected to differ with geologies, thus it is no wonder that slag composition varies remarkably across locations. Any change in the composition of raw material and/or in the furnace passage affects the composition of slag. Besides, different blast furnace management and metallurgical technology change slag chemistry further [4, 5]. Researchers in [6, 7] reviewed the chemistry of various SCMs, of which slag was located between Portland cement and fly ash.

As a result, the intrinsic reactivity of slag, depending on parameters, e.g. chemical composition in particular, glass content, etc. also fluctuates significantly. Generally, slag reactivity increases with the increasing CaO, Na_2O, and K_2O contents, and with the decreasing amounts of SiO_2, FeO/Fe_2O_3, TiO_2, MnO/Mn_2O_3, etc. [8–14]. A high CaO/SiO_2 ratio indicates a good reactivity, and a deficiency in CaO can be compensated by MgO, as stated in European standard EN 15167-1. Moreover, increased Al_2O_3 content of slag was reported to enhance reaction heat release and early age strength development [13, 15]. Due to the higher molar volume of Al-containing phases, e.g. ettringite and calcium monosulfoaluminate (*monosulfate* for short), these hydrates can fill up pores and are thus beneficial for the compressive strength development [16]. In the work of [17], the authors confirmed a positive correlation between Al_2O_3 content of slag and reactivity.

As for the carbonation rate of cement-slag system, it is generally recognized higher than that of Ordinary Portland cement system with the same water/binder ratio, partially owing to its lower calcium hydroxide content [18–22]. Portlandite, as the main CO_2 buffer phase, can delay the decalcification of the most essential hydration product in cement matrix, i.e. the $C-S-H$ gel phase [19, 23, 24]. For various blended cement pastes, $C-S-H$ gel phase with a typically lower Ca/Si atomic ratio is produced, which is more easily carbonated, reaching a critical Ca/Si ratio of 0.67 [25–27]. This kind of silica gel is poorly organized and presents a low molar volume, certainly leading to an increase in porosity and destroying the microstructure of system subsequently. On the other hand, much attention has been paid to the carbonation behavior of portlandite and $C-S-H$ gel phase

*Corresponding author. Email: Y.Zhang-28@tudelft.nl

© 2023 The Author(s). Published by Informa UK Limited, trading as Taylor & Francis Group
This is an Open Access article distributed under the terms of the Creative Commons Attribution License (http://creativecommons.org/licenses/by/4.0/), which permits unrestricted use, distribution, and reproduction in any medium, provided the original work is properly cited. The terms on which this article has been published allow the posting of the Accepted Manuscript in a repository by the author(s) or with their consent.

in the past decades, while few studies dug deep into the carbonation of minor hydration phases, e.g. ettringite, monosulfate, and hydrotalcite-like phase. In other words, the role of slag (even in slag-rich mixtures, e.g. CEM III/B) as well as its hydration products during carbonation have been largely neglected. As stated in [24], understanding the role of minor hydrates in the carbonation process was imperative if next-generation binders are to be designed to favor formation of specific microstructural features to maximize their carbonation resistance.

In our previous study [28], the authors revealed the effect of MgO content in slag on the carbonation characteristics of slag-rich cement paste, where it was found that the carbonation resistance improved notably with the increasing MgO content in slag, in which hydrotalcite-like phase played a key role. However, questions such as whether Al_2O_3-rich slag also contributed to the improvement of carbonation resistance and whether slag reactivity indicated by, e.g. R3 test can be extended to characterize carbonation resistance of slag-rich blends etc. remained to be answered. Therefore, the present study attempted to fill up these gaps by investigating the influence of Al_2O_3 content in slag on the relationship between slag reactivity and carbonation resistance

In the work of [17], hydraulicity test (R3 test) based on a model system and dissolution test in a NaOH solution were already used to investigate the effect of slag chemistry on reactivity systematically. These synthetic slags were further considered in the current study, where slag was adopted as a primary SCM (i.e. 70 wt.% replacement level), and the influence of slag chemistry on carbonation resistance of slag-rich cement was studied. The evolution of phase assemblage and microstructure development before and after accelerated carbonation testing were examined, and the CO_2 binding capacity of each mixture was compared. Under this circumstance, a snapshot depicting the interaction among slag chemistry, reactivity, and carbonation characteristics of slag-rich cement can be obtained, and the authors are thus able to answer whether slag reactivity can be used as an indicator, building the correlation between slag chemistry and carbonation resistance of slag-rich cement.

2. Materials and methodology

2.1. Materials

CEM I 42,5 N, manufactured by ENCI Maastricht B.V., was used in this study to produce cement-slag binary blends. Synthetic slags with different Al_2O_3 contents, were produced in the laboratory. The synthetic slag was prepared by mixing analytical reagents including CaO, SiO_2, Al_2O_3, and MgO according to different compositional design targets. The analytical reagents added to control the exact composition in each run were mixed into a homogeneous blend by combining the materials with pure ethyl alcohol, grinding the mixture in a ball milling machine at a low speed for 2 h and drying them at 100 °C for 24 h. The dried material was then ground to finer than 200 μm using a mortar and pestle for improved homogeneity. Then, it was melted in an Al_2O_3 crucible at 1550 °C in the oven (High temperature furmace, Carbolite) for 3 h (heated from room temperature to 1550 °C at 10 °C/min and maintained at 1550 °C for 3 h). The molten liquid was water quenched to obtain glassy slag, rinsed with isopropanol and dried at 100 °C for 24 h, subsequently. Finally, it was crushed and ground down to the required particle size distribution in a ball mill (Retsch PM 100).

Chemical compositions measured by X-ray fluorescence (XRF) of cement and slags are presented in Table 1. Figure 1 illustrates the particle size distribution of slags and quartz tested by laser diffraction. For synthetic slag A3, A12 and A18, CaO/SiO_2 ratio was maintained at around 1.0 and the amount of MgO was stabilized at about 9 wt.%, while Al_2O_3 content was increased from 3.69 to 18.19 wt.%. As for synthetic slag CS1 and CS2, their Al_2O_3 contents were maintained at a high level, i.e. 14.51

Table 1. Chemical compositions (wt.%) and physical properties of CEM I 42,5 N and synthetic slags.

	Cement	A3	A12	A18	CS1	CS2
CaO	64	42.07	37.32	36.87	***32.98***	***28.05***
SiO_2	20	43.30	39.11	34.43	***38.67***	***42.84***
Al_2O_3	5	***3.69***	***12.32***	***18.19***	***14.51***	***17.12***
MgO	—	10.83	9.43	7.98	11.22	9.67
FeO/Fe_2O_3	3	0.07	0.30	0.40	0.36	0.35
TiO2	—	—	0.70	0.84	1.02	0.89
MnO/Mn_2O_3	—	—	0.15	0.27	0.22	0.19
Na_2O_{eq}[a]	0.58	—	0.38	0.64	0.60	0.52
SO_3	2.93	0.01	0.03	0.03	0.05	0.08
Residual	4.49	0.03	0.19	0.21	0.25	0.08
CaO/SiO_2	—	0.97	0.95	1.07	0.85	0.65
$(CaO + MgO)/SiO_2$[b]	—	1.22	1.20	1.30	1.14	0.88
Physical properties						
d_{50} (μm)[c]	26.81	19.67	20.35	20.85	20.40	20.11
SSA (m^2/g)[d]	0.284	1.09	0.92	0.90	0.93	1.08

[a]The Na_2O_{eq} employed here for cement and slag was identical, namely $Na_2O + 0.658*K_2O$.
[b]The European Standard EN 15167-1 recommends that this ratio should be greater than 1.
[c]The particle size distribution (PSD) of slag was measured by EyeTech, Ankersmid. The d_{50} of quartz was 24.21 μm.
[d]The specific surface area (SSA) of cement and slag was measured by Blaine and nitrogen adsorption with the BET method, respectively.

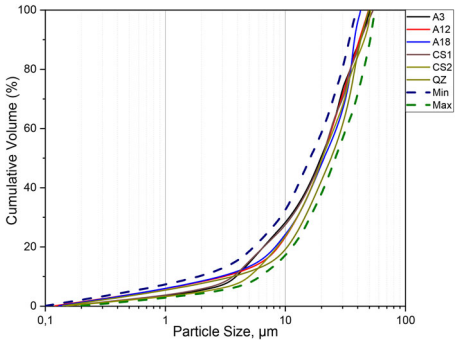

Figure 1. Particle size distribution of synthetic slags and quartz.

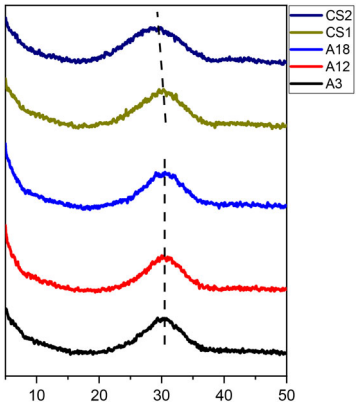

Figure 2. XRD scans of synthetic slags used in the present research.

and 17.12 wt.%, respectively, while the CaO/SiO_2 ratios were reduced to less than 1.0. The main target of inclusion slag CS1 and CS2 was to investigate whether high alumina content in slag can compensate the negative effect of reduced CaO/SiO_2 ratio.

X-ray diffraction (XRD) scans of five synthetic slags are shown in Figure 2, which were almost entirely amorphous with no peak indicating the existence of a crystal phase. It was noticed that the position of amorphous hump shifted small quantity to the left as the CaO/SiO_2 ratio decreased. Similarly, the position also shifted slightly to a smaller angle with decreasing $CaO + MgO$ content (i.e. increasing Al_2O_3 content).

2.2. Mix design and methodology

Quartz (Qz) with a similar PSD was also introduced to cast cement-quartz paste, acting as a reference. In the blended cement paste, cement clinker was partially replaced by slag or quartz (70%). Paste specimens were prepared in each mixture using distilled water with a water/binder (cement + slag/quartz) ratio of 0.40. All the materials were in mass percentage with respect to total binder content. To avoid the introduction of extra interferences, sulfate content in cement was not adjusted to account for the variations of alumina in slags (especially for slag A18 and CS2 with high Al_2O_3 contents), which might change the phase assemblage of mixtures at early age [29–31]. The binders were mixed and then transferred immediately to the molds ($40 \times 40 \times 40$ mm). After one day, specimens were demoulded and cured in sealed condition at 20 ± 2 °C (room temperature) until further investigation.

After 3 months of curing when it was assumed that the hydration had reached an equilibrium, specimens were transferred to a relative humidity (RH)-controlled climate chamber at 65% and 20 °C for pretreatment for one month, as suggested by [32]. Accelerated carbonation test was performed in an accelerated carbonation chamber (Wewon Tech) sequentially regulated by CO_2 concentration of 3 vol.% ± 0.2, at 20 ± 3 °C and 65 ± 5% of RH (using saturated $NaNO_2$ solution). Only one surface of the specimens was exposed to CO_2 and the other surfaces were sealed to ensure one dimensional diffusion. The carbonation process continued up to 6 months to ensure that CO_2 had entered the pastes as much as possible.

At the end of the predesignated hydration and carbonation periods, small disks were cut from the specimens, crushed and immersed in isopropanol solution to exchange free water. Prior to XRD measurement and thermogravimetric analysis (TGA), the crushed slices were dried at 40 °C, ground with mortar and sieved manually to obtain particle size below 63 μm. XRD data was collected using a Philips PW 1830/40 Powder diffractometer with Cu K-alpha radiation. The machine was operated with an X-ray beam current of 40 mA and an acceleration voltage of 40 kV. These sample powders were scanned from 5 to 60° (2θ) with a step size of 0.03°. Netzsch STA 449 F3 Jupiter coupled with mass spectrometer (MS) Netzsch QMS 430 C was employed for thermogravimetric analysis. The emission of H_2O and CO_2 was thus identified. A powder sample of approx. 50 mg was heated under an argon atmosphere with a heating rate of 10 °C/min from 40 to 800 °C in an Al_2O_3 crucible, with an identical and blank one as reference. Moreover, the CO_2 response of samples with unknown CO_2 concentrations was calibrated with the response of a standard (pure $CaCO_3$ reagent, VWR Chemicals BDH) with known CO_2 concentration (44.0 wt.%) under the same analytical condition. This method allowed the quantification of CO_2 emission from carbonated slag cement paste in the present study containing both calcium carbonate and other CO_2 binding phases. The area under the MS CO_2 curve, or peak integral, was calculated with OriginPro 2019, a commercial software.

Fourier transform infrared spectroscopy (FTIR) was performed using Spectrum TM 100 Optical ATR-FTIR spectrometer over the wavelength range from 600 to 4000 cm^{-1} to characterize the alteration of molecule structure before and after accelerated carbonation test. A single-beam configuration was used, and each sample was scanned 20 times with a fixed instrument resolution of 4 cm^{-1}.

Mercury intrusion porosimetry (MIP) analysis was performed with a Micromeritics Autopore IV which determined pore size down to 7 nm (corresponding to a 0–210 MPa range of applied pressure). Diminished particles were immersed in isopropanol solution to stop hydration. They were subsequently stored in a desiccator under vacuum to remove the isopropanol. The Washburn equation

explains the relationship between pore diameter (D) and pressure (P) as the below formula shows,

$$P = -\frac{4\gamma\cos(\theta)}{D}$$

of which the surface tension of mercury (γ) is 0.485 N/m at 25 °C and the contact angle (θ) between mercury and sample is 140°. Three steps were involved in each measurement process, i.e. mercury intrusion at low pressure from 0 to 0.170 MPa; at high pressure from 0.170 to 210 MPa; and mercury extrusion.

Slices of hydrated specimens were also used in the scanning electron microscopy (SEM) investigation. After stopping hydration, the specimens were impregnated with a low viscosity epoxy resin and mirror polished using polishing diamond paste down to 0.25 μm. The samples were further coated with carbon and examined with a FEI QUANTA FEG 650 ESEM instrument under a 10 kV accelerating voltage and a working distance of 10 mm. Micrographs were acquired using backscattered electron (BSE) detector. X-ray energy dispersive spectrometry (EDS) was also used to determine the elemental composition of the phase assemblages. Approximately 100 points per sample were microanalyzed at the matrix and slag rims.

Thermodynamic modeling was carried out to investigate the effect of Al_2O_3 content of slag on the carbonation characteristics using the Gibbs free energy minimization program GEMS [33, 34] with thermodynamic data from the PSI-GEMS database [35, 36] supplemented by cement specific data [37, 38]. The calcium-alkali aluminosilicate hydrate ideal solid solution model (CNASH_ss) proposed by Myers et al. [39] was employed to describe the C – S(A)–H gel phase in the system. MgAl – OH – LDH_ss containing three end-members with Mg/Al atomic ratios of 2, 3 and 4 reformulated into an ideal solid solution was considered to simulate the formation of hydrotalcite–like phase before carbonation [40]. For their corresponding carbonation forms, the database provided by [41] was incorporated in the model as candidate phases. The thermodynamic properties of these carbonated forms were calculated based on the ion-exchange constant provided by [42].

3. Results

3.1. Phenolphthalein spray

The typical cross-sectional surfaces of the specimens after phenolphthalein spray are shown in Figure 3. It was noted that slag A3, A12, A18, and CS1 pastes exhibited similar carbonation depths in the range of 10–15 mm. On the other hand, the carbonation depth of slag CS2 paste was approximately 20 mm, significantly higher than others.

3.2. Carbonation products

In this section, the authors characterized carbonation products by means of a series of techniques. To better understand the effect of CO_2 attack on the evolution of phase assemblage, powders were taken from the top layer of specimens (within 3 mm depth from the surface) exposed in the carbonation chamber to ensure full carbonation as much as possible.

3.2.1. Thermogravimetry (TG-DTG-MS)

Figure 4(a) reveals the representative TG-DTG results of cement-slag and quartz mixtures at 90 days of curing. The peak at 400–500 °C indicated the formation of portlandite. Expectedly, the most portlandite was identified in cement-quartz blend while the least amount of portlandite was found in slag A18 mixture due to its relatively high reactivity [17]. Hydrotalcite-like phase was detected in slag-containing mixtures with a distinct peak located at approximately 350 °C. Additionally, the shoulder at ~200 °C implied the formation of monosulfate, originated from the transformation of ettringite with time. Note that its amount was positively associated with the amount of alumina content in slag, i.e. nearly no monosulfate was found in slag A3 blend while slag A18 mixture presented the most distinct shoulder at ~200 °C. Meanwhile, the peak at 100–150 °C suggested the presence of C – S–H gel phase.

Figure 4(b-1)–(b-4) show the DTG results, H_2O and CO_2 MS curves of fully carbonated cement-slag A3, CS1, A18, and Qz pastes, respectively. No doubt that the main CO_2-bearing phase in all pastes was calcium carbonate, and three decomposition peaks starting from ~450 °C in the DTG graph implied the presence of amorphous

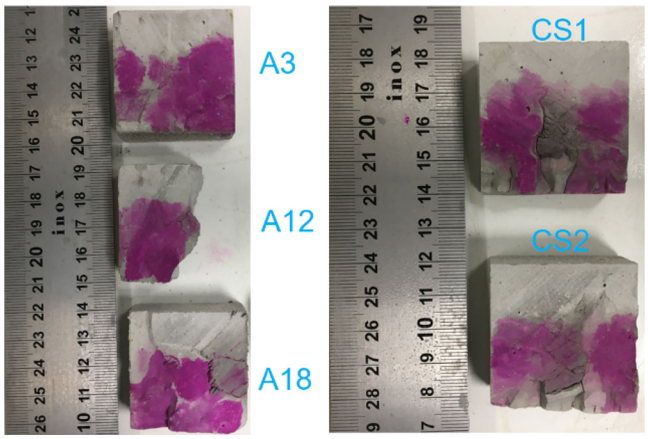

Figure 3. Typical sawn surfaces of the specimens after spraying with phenolphthalein solution.

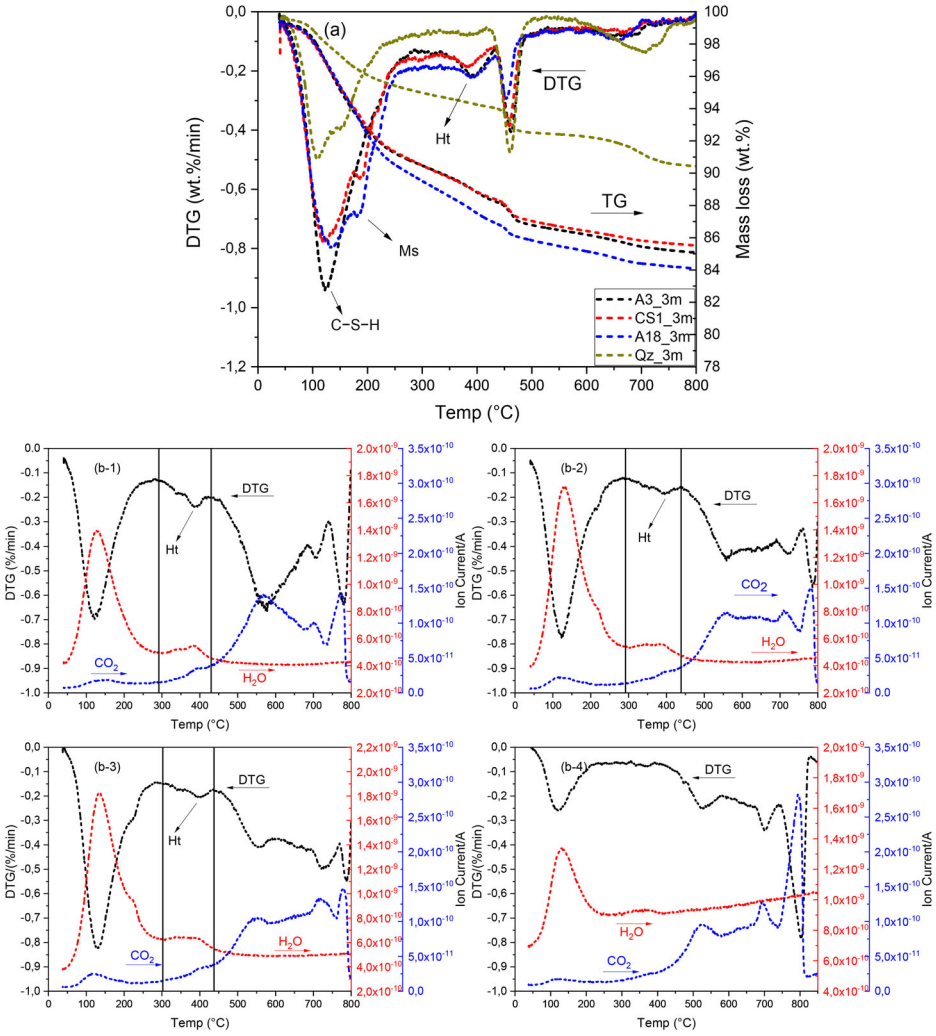

Figure 4. (a) TG and DTG results of representative cement-slag and quartz mixtures after 3 months of curing; (b-1) to (b-4) DTG results, H_2O and CO_2 MS curves of fully carbonated cement-slag A3, CS1, A18, and Qz pastes, respectively. Ht: hydrotalcite-like phase; Ms: calcium monosulfoaluminate.

calcium carbonate, vaterite, and calcite correspondingly, all of which were commonly seen in the accelerated carbonation test of cementitious materials [43, 44]. Also, the carbonates in the carbonated quartz blend started decomposing at a lower temperature than that in the slag cement pastes, which was indicative of the carbonation C − S−H gel phase [45]. Monosulfate and portlandite had been carbonated and decomposed completely, as neither of them was observed in the fully carbonated area.

The peak located at 300–450 °C indicated the persistence of hydrotalcite-like phase after carbonation in slag-containing blends. As displayed in the MS curves, both H_2O and CO_2 were released at this temperature range. Considering the stacked layers structure of this phase [42], it implied that CO_2 was absorbed in the interlayer space to replace water molecules absorbed originally, to form the carbonated phase. Moreover, a small peak at ∼150 °C occurred in the MS CO_2 curve, irrespective of the addition of slag or Al_2O_3 content of slag. It can be ascribed to the release of CO_2 from carbonated Ca-Al AFm phases (amorphous or nano-crystalline), sourced from the carbonation of AFm-OH and/or AFm-SO_4 phases [46], or forming carbonate-sulfate AFm solid solution [47]. This peak was negligible in slag A3 and Qz mixtures, probably owing to their reduced monosulfate formation after hydration when compared with other pastes.

3.2.2. *X-ray diffraction (XRD)*

XRD results (Figure 5(a)) confirm the presence of monosulfate, hydrotalcite-like phase, portlandite, and unhydrated cement clinker (C_3S and β-C_2S in particular) in slag cement paste after hydration. The peak intensity of portlandite reduced with the gradual addition of Al_2O_3 in slag. Monosulfate was detected in slag A12 and A18 mixtures. On the other hand, the peak for monosulfate and portlandite disappeared in all mixtures after carbonation (Figure 5(b)). These results were consistent with the TGA findings (Figure 4). Moreover, it was found that the peak for unhydrated cement clinkers (C_3S and β-C_2S) also disappeared in the fully carbonated area, likely due to the continuation of hydration or carbonation [48].

Hydrotalcite-like phase was still detected after such a heavy CO_2 attack, i.e. the peak of which was located at ∼11° both before and after carbonation. Calcite and vaterite were identified as the main polymorphs of calcium

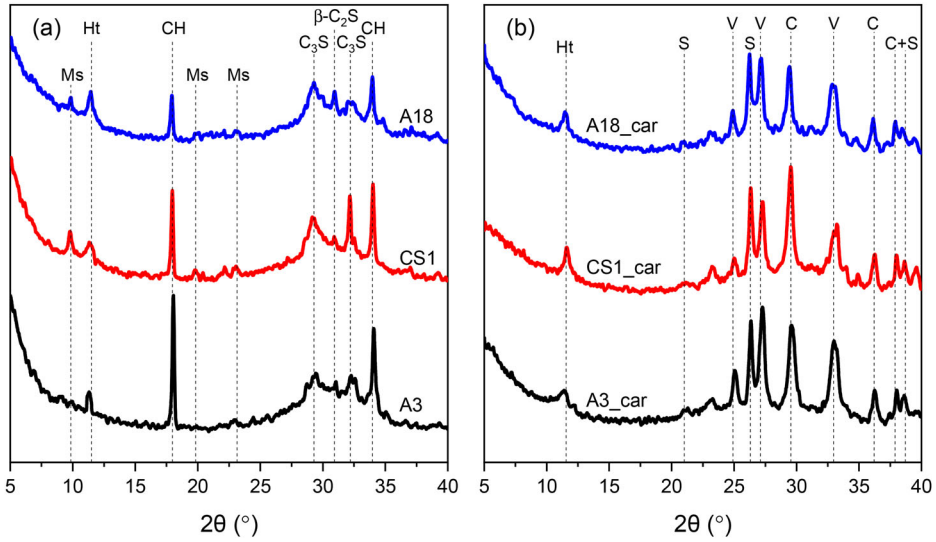

Figure 5. XRD analysis of representative cement-slag blends (a) at 90 days after curing; (b) after full carbonation. Ms: calcium monosulfoaluminate; Ht: hydrotalcite-like phase; CH: portlandite; C: calcite; V: vaterite. The peak centered at around $2\theta = 21$ and 26° appeared to be associated with the formation of silica gel (labeled as S) due to the carbonation of C – S – H gel phase [20].

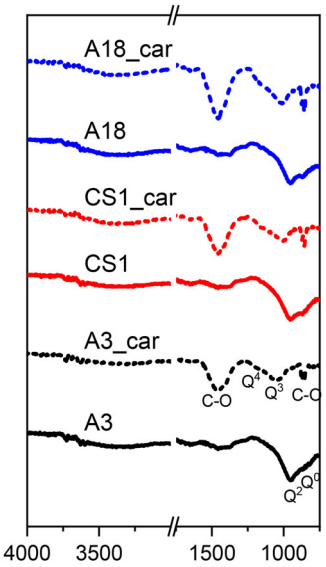

Figure 6. FTIR spectra of slag cement pastes after 3 months of curing and accelerated carbonation test.

carbonate. It is worth mentioning here that amorphous calcium carbonate could not be detected by XRD and no trace of aragonite was confirmed in these carbonated samples.

3.2.3. *Fourier transform infrared (FTIR) spectroscopy*

As Figure 6 shows, FTIR spectra of slag cement pastes presented similar characteristics after 3 months of curing, and Q^2 (~950 cm^{-1}) was the main unit of C – S–H gel phase of all investigated mixtures before carbonation. Moreover, the silicate group in these samples also showed a similar feature after carbonation, i.e. the Si-O-T stretching band shifted to higher wavenumbers in the range of ~1200 and ~1100 cm^{-1}, indicating the formation of Q^4 and Q^3 silicate units, respectively. This shift was associated with the gradual polymerization of silicate units, namely the carbonation-induced decalcification of C – S–H gel phase [49].

The strong broad band at 1400–1500 cm^{-1} and narrow band at 875–1000 cm^{-1}, representing the asymmetric stretching and bending of carbonate, respectively further confirmed the reaction with CO_2 and production of CO_3 band [50].

Collectively, the variation of slag chemistry did not change the type of carbonation products of slag cement fundamentally, and three CO_2 binding phases were identified, i.e. calcium carbonate (including amorphous calcium carbonate, vaterite, and calcite), carbonated hydrotalcite-like phase, and carbonated Ca-Al AFm phases (These phases cannot be detected by XRD.). The formation of silica gel after carbonation was confirmed by both XRD and FTIR.

3.3. *Degree of CO_2 uptake of different carbonate phases*

To calculate the CO_2 concentration in each carbonate phase at different depths, powders were extracted from the regions with different degrees of carbonation. These regions were designated as: (nearly) fully carbonated zone (label 1), transitional/dissolution zone (label 2) [51], and mildly/non-carbonated area (label 3), respectively as Figure 7 shows.

Figure 8(a) and (b) display the DTG results, H_2O and CO_2 MS curves of the powders taken from mildly carbonated and transitional areas of slag A18 paste, respectively (For fully carbonated area, it was shown in Figure 4(b-3)). The carbonation degree in these two areas was lower than that in full carbonation area, indicated by the reduced CO_2 ion current. Nonetheless, the same carbonate phases can be identified in these three areas, i.e. carbonated Ca-Al AFm phases, carbonated hydrotalcite-like phase as well as calcium carbonate. Additionally, portlandite was observed in the transitional area while both portlandite and monosulfate were detected in the mildly carbonated area.

Pure $CaCO_3$ reagent was employed as a reference to calibrate the CO_2 content in each carbonate paste under

the same analytical condition. Figure 9(a) presents the DTG result, CO_2 MS curve of pure $CaCO_3$. The area under the MS CO_2 curve corresponding to 44.0 wt.% CO_2 releasing from $CaCO_3$ was calculated with commercial software OriginPro 2019.

As confirmed in section 3.2, calcium carbonate existed in polymorphs after carbonation. They started to decompose from ~500 °C and the decomposition peaks overlapped with each other noticeably [32, 43, 44]. However, the simultaneous presence of these polymorphs did not affect the determination of total CO_2 bound in calcium carbonate. As for carbonated hydrotalcite-like phase, it released CO_2 at 250–450 °C, and an apparent decomposition peak was noted in this temperature range [52]. Fortunately, no other phases released CO_2 within this range in the carbonated slag cement sample. Therefore, the CO_2 concentration of each carbonate phase at different depths can thus be estimated from the area under the CO_2 MS curve in the corresponding temperature range, using slag A18 paste as an example shown in Figure 9(b–d). The areas A1, A2 and A3 were related to certain amounts of CO_2 liberated from carbonated Ca-Al AFm phases, carbonated hydrotalcite-like phase, and calcium carbonate, respectively.

The calculated areas under the MS CO_2 curve and CO_2 concentrations calibrated with pure $CaCO_3$ (/100 g carbonated paste) of different carbonate phases in each mixture are given in Tables 2 and 3, respectively. No doubt that the absolute amount of CO_2 bound in different carbonate phases increased significantly from mildly to fully carbonated area. Moreover, it can be seen that

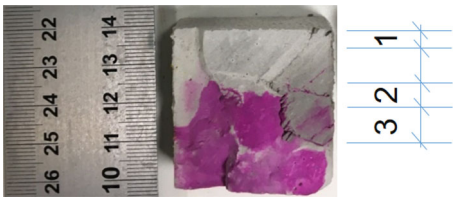

Figure 7. The positions where powders were extracted, using slag A18 paste as an example. 1: fully carbonated area; 2: transitional area; 3: mildly carbonated area.

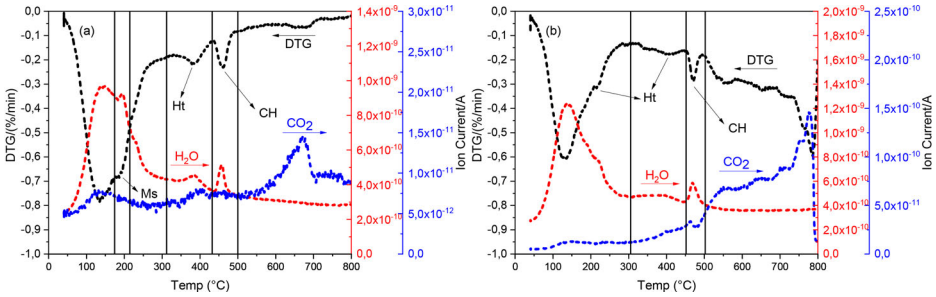

Figure 8. DTG results, H_2O and CO_2 MS curves of (a) mildly carbonated and (b) transitional areas of slag A18 paste, respectively. Ms: calcium monosulfoaluminate; Ht: hydrotalcite-like phase; CH: portlandite.

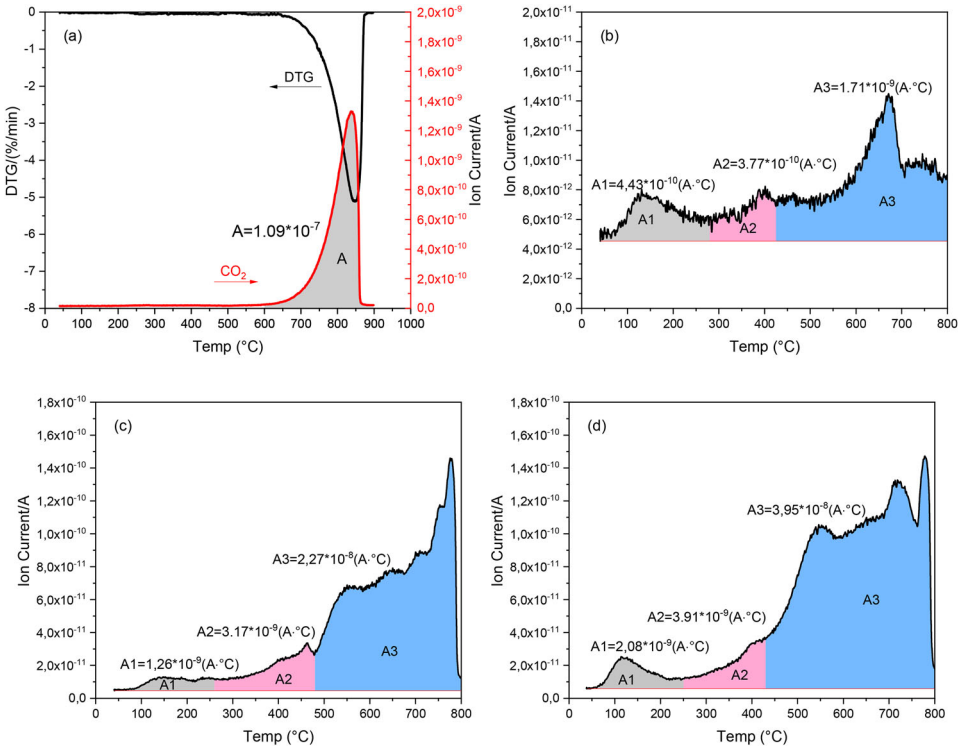

Figure 9. (a) The DTG result, CO_2 MS curve of pure $CaCO_3$; (b-d) The CO_2 MS curve of carbonated slag A18 paste from mildly carbonated, transitional, and fully carbonated areas, respectively.

Table 2. The calculated area under the MS CO_2 curve of different carbonate phases (A·°C).

		Area under the MS CO_2 curve			
		Carbonated Ca-Al AFm phases	Carbonated hydrotalcite-like phase	Calcium carbonate	Total
Mildly carbonated	A3	$7.39*10^{-10}$	$1.02*10^{-9}$	$2.97*10^{-9}$	$4.73*10^{-9}$
	A12	$6.50*10^{-10}$	$9.68*10^{-10}$	$2.81*10^{-9}$	$4.43*10^{-9}$
	A18	$4.43*10^{-10}$	$3.77*10^{-10}$	$1.71*10^{-9}$	$2.53*10^{-9}$
	CS1	$4.12*10^{-10}$	$8.63*10^{-10}$	$2.68*10^{-9}$	$3.96*10^{-9}$
	CS2	$5.39*10^{-10}$	$9.35*10^{-10}$	$2.84*10^{-9}$	$4.13*10^{-9}$
Transitional	A3	$1.23*10^{-9}$	$3.17*10^{-9}$	$2.05*10^{-8}$	$2.49*10^{-8}$
	A12	$1.71*10^{-9}$	$3.89*10^{-9}$	$2.56*10^{-8}$	$3.12*10^{-8}$
	A18	$1.26*10^{-9}$	$3.17*10^{-9}$	$2.27*10^{-8}$	$2.71*10^{-8}$
	CS1	$1.43*10^{-9}$	$3.35*10^{-9}$	$2.31*10^{-8}$	$2.79*10^{-8}$
	CS2	$1.52*10^{-9}$	$3.46*10^{-9}$	$2.38*10^{-8}$	$2.88*10^{-8}$
Fully carbonated	A3	$1.56*10^{-9}$	$2.84*10^{-9}$	$3.94*10^{-8}$	$4.38*10^{-8}$
	A12	$1.94*10^{-9}$	$5.11*10^{-9}$	$3.73*10^{-8}$	$4.43*10^{-8}$
	A18	$2.08*10^{-9}$	$3.91*10^{-9}$	$3.95*10^{-8}$	$4.55*10^{-8}$
	CS1	$1.74*10^{-9}$	$4.25*10^{-9}$	$3.72*10^{-8}$	$4.32*10^{-8}$
	CS2	$1.83*10^{-9}$	$4.87*10^{-9}$	$3.85*10^{-8}$	$4.52*10^{-8}$
	Qz [a]	$1.50*10^{-9}$	—	$3.81*10^{-8}$	$3.96*10^{-8}$
	Pure $CaCO_3$	—	—	$1.09*10^{-7}$	$1.09*10^{-7}$

Table 3. CO_2 concentration of different carbonate phases calibrated with pure $CaCO_3$ (/100 g).

		CO_2 concentration of each carbonate phase			
		Carbonated Ca-Al AFm phases	Carbonated hydrotalcite-like phase	Calcium carbonate	Total
Mildly carbonated	A3	0.30	0.41	1.20	1.91
	A12	0.26	0.40	1.13	1.79
	A18	0.18	0.15	0.69	1.02
	CS1	0.17	0.35	1.08	1.60
	CS2	0.23	0.39	1.15	1.67
Transitional	A3	0.50	1.28	8.27	10.05
	A12	0.69	1.57	10.33	12.59
	A18	0.50	1.28	9.16	10.94
	CS1	0.58	1.35	9.33	11.26
	CS2	0.62	1.40	9.61	11.63
Fully carbonated	A3	0.63	1.15	15.90	17.68
	A12	0.78	2.06	15.04	17.88
	A18	0.84	1.58	15.95	18.37
	CS1	0.70	1.72	15.02	17.44
	CS2	0.74	1.97	15.54	18.25
	Qz	0.51	—	15.38	15.99
	Pure $CaCO_3$	—	—	44.0	44.0

calcium carbonate bound the majority of CO_2 diffused into the paste, by the reactions between portlandite as well as C − S−H gel phase and CO_2. Meanwhile, the CO_2 binding capacity (full carbonation) of each mixture was similar, and it fluctuated at 15–20 wt.% in the completely carbonated area, irrespective of alumina content in slag.

3.4 Microstructure

In this section, the authors aimed to analyze the impact of carbonation on the microstructure development and the evolution of phase assemblages in the cement-slag systems. Samples used for measurements were selected from the carbonated area (colorless appearance after phenolphthalein spray) for each mixture.

3.4.1. MIP

As Figure 10(a) illustrates, the critical pore diameter of cement-slag system fluctuated at around 0.01 μm, and it exhibited a decreasing trend with the increasing Al_2O_3 content of slag. Slag CS1 and CS2 pastes exhibited a relatively larger critical pore diameter between 0.01 and 0.02 μm due to the decreased CaO/SiO_2 ratio. Compared with cement-quartz mixture which displayed a bimodal pore structure (in the range of 0.01–1 μm), secondary precipitations from the pozzolanic reaction between portlandite and slag helped refine and densify the pore structure of paste considerably.

After accelerated carbonation test, the critical pore diameter of each mixture all increased to the range of 0.1–10 μm (Figure 10(b)). Due to the carbonation of C − S−H gel phase, a much coarser pore structure was produced

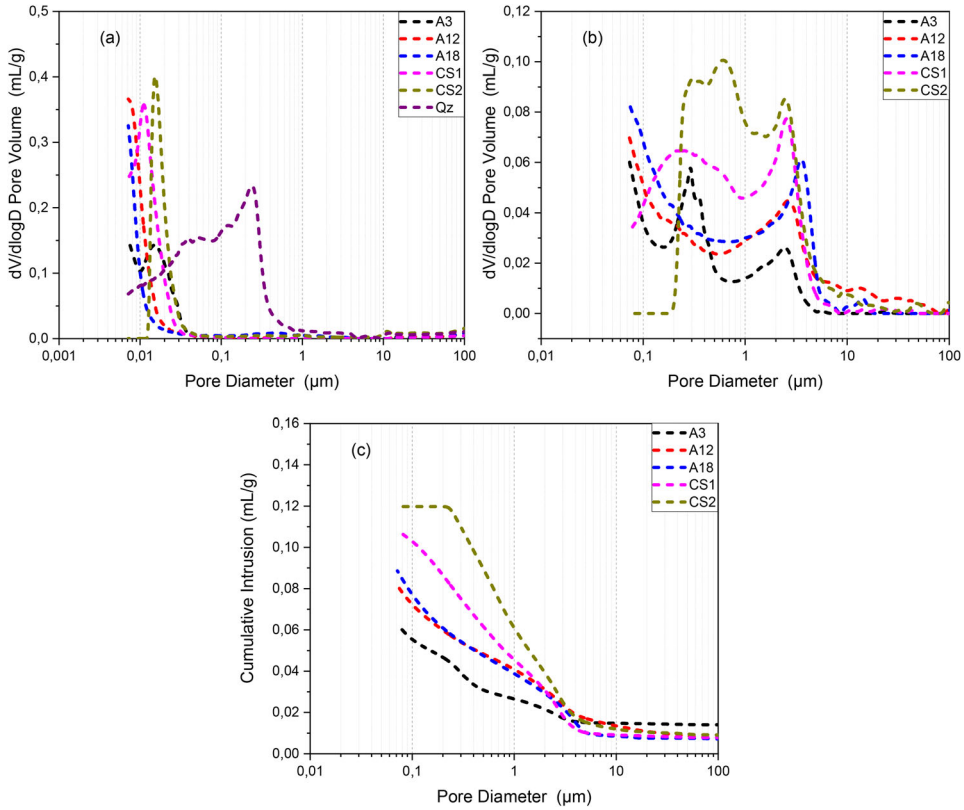

Figure 10. Differential pore size distribution of cement-slag and quartz mixtures measured (a) before and (b) after accelerated carbonation test; (c) cumulative intrusion measured after accelerated carbonation test.

after carbonation. The decalcification of C – S–H gel phase produced a poorly organized silica gel of a lower molar volume. At the same time, free water initially bound within the C – S–H gel phase was released during carbonation and evaporated with drying, which also contributed to an enhanced porosity [20, 53, 54]. It was also noted that slag A12 and A18 pastes showed a similar critical pore diameter (Figure 10(b)) and porosity (Figure 10(c)) after carbonation, while slag CS1 and CS2 blends illustrated the most porous microstructure during CO_2 attack.

3.4.2. SEM-BSE

To keep consistent with Section 3.2, Figure 11 illustrates the representative microstructures of specimens before and after accelerated carbonation test. Unhydrated cement grains (e.g. circled and labeled 1 in Figure 11(a-1)) were found in all pastes and distributed in the matrix with unhydrated slag particles after 3 months of curing. Portlandite was clearly identified as large clusters (e.g. circled and labeled 2 in Figure 11(a-1)). Because of the rich alumina content in slag A18, monosulfate existed as fine and compact crystal intermixed with C – S–H gel phase across the matrix (circled and labeled 3 in Figure 11(c-3)).

After carbonation, specimens appeared much more porous with a large quantity of black spots, indicating the formation of pores filled with epoxy resin (Figure 11(a-2) to (c-2)). It further verified the change in critical pore radii upon carbonation in the range of 0.1–10 μm measured by MIP.

3.4.3. Chemical composition

3.4.3.1. C – S – H Gel phase. Scatter plots of Al/Ca against Si/Ca in atomic ratio are shown in Figure 12. In general, the measured Ca/Si atomic ratio of C – S–H gel phase after 3 months of curing fluctuated at around 1.0. This value was in line with the earlier reports [55]. On the other hand, substantial decalcification occurred in the blended system after accelerated carbonation testing which led to a reduction of Ca/Si atomic ratio of C – S–H gel phase. Several Ca/Si ratio readings were similar to that of uncarbonated gel matrix, probably related to the intermixing of carbonates. The other part was decalcified, especially for that circled in Figure 12(b). Moreover, scatter points indicating the existence of monosulfate in slag A18 mixture disappeared after carbonation, confirming the decomposition of this phase after carbonation.

3.4.3.2. Hydrotalcite-like phase. Consistent with the results in [56], hydrotalcite-like phase seemed to be unaffected by CO_2 attack. The Mg/Al atomic ratio derived from the regression analysis of Mg/Si against Al/Si scatter plot (Figure 13) remained nearly unchanged before and after carbonation. In other words, hydrotalcite-like phase remained intact during carbonation, and the CO_2 uptake in

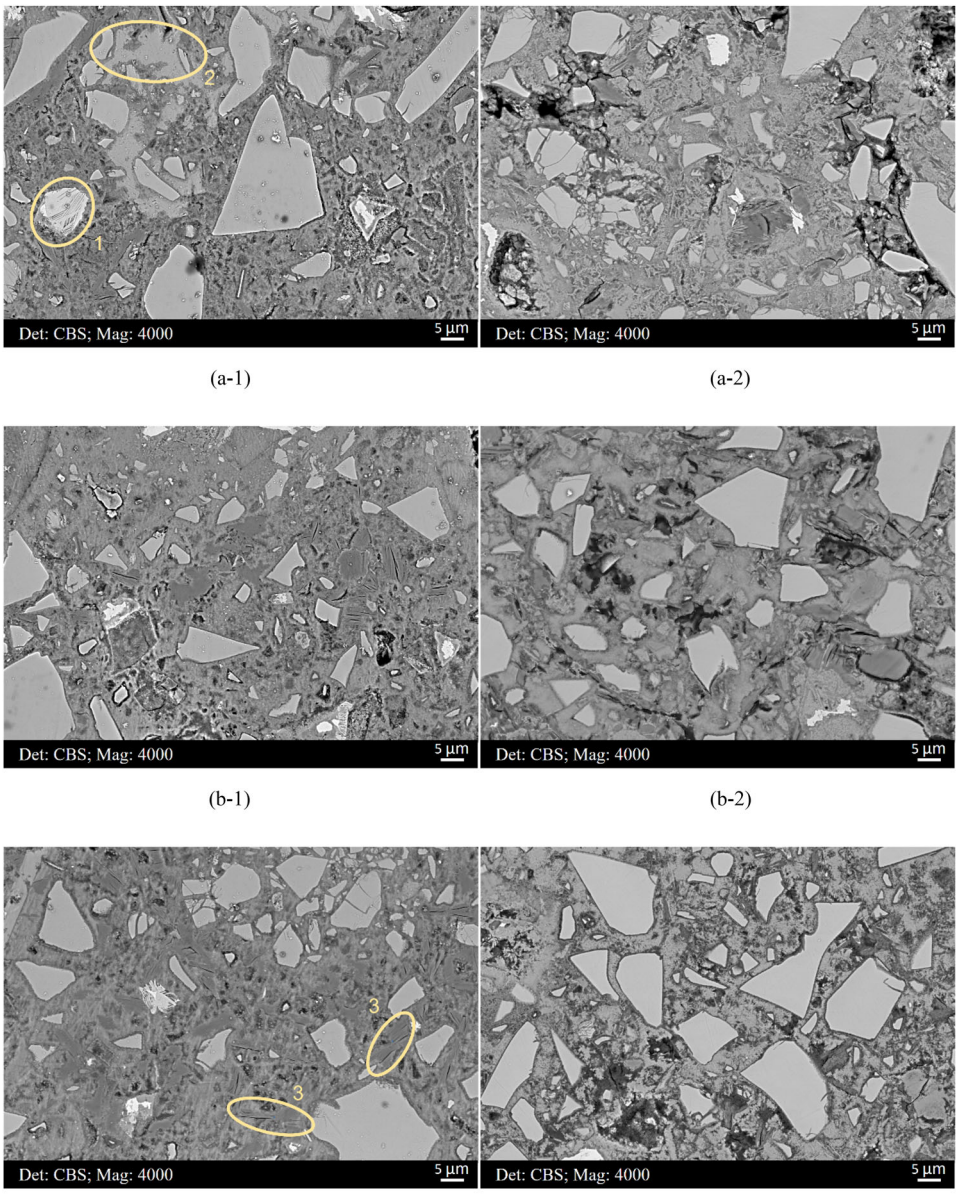

(a-1) (a-2)

(b-1) (b-2)

(c-1) (c-2)

Figure 11. Microstructure of (a-1) to (c-1) cement-slag A3, CS1, and A18 mixtures after curing of 3 months, respectively; and (a-2) to (c-2) carbonated area of cement-slag A3, CS1, and A18 mixtures, respectively.

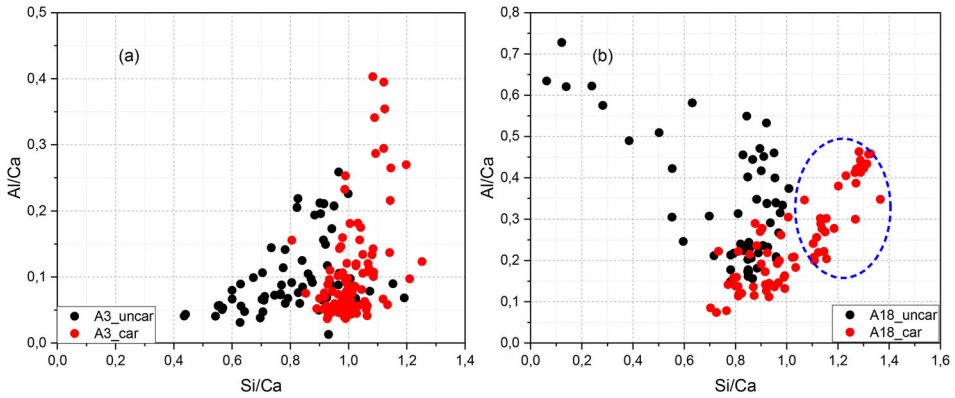

Figure 12. Representative plots of Al/Ca against Si/Ca in atomic ratio of slag (a) A3 and (b) A18 pastes before and after carbonation.

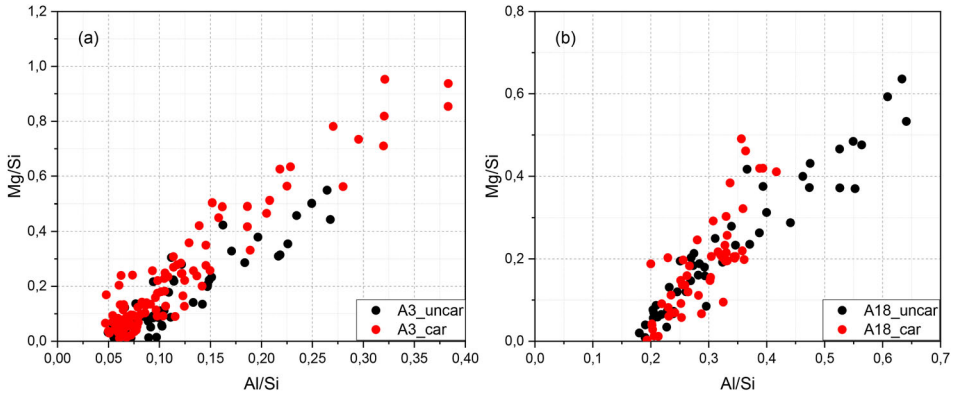

Figure 13. Representative plots of Mg/Si against Al/Si in atomic ratio of slag (a) A3 and (b) A18 pastes before and after carbonation.

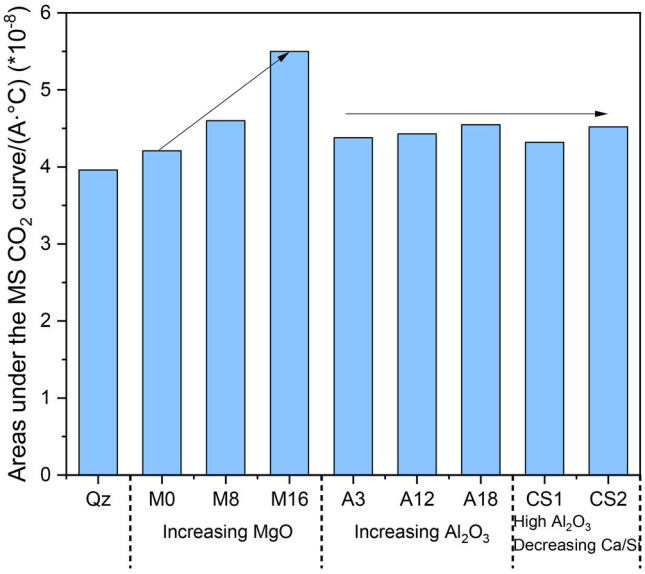

Figure 14. The areas under MS CO_2 curves or CO_2 binding capacity against slag chemistry.

its interlayer space would not decompose its network structure.

4. Discussion

4.1. *Slag chemistry vs. CO_2 binding ability*

It is well recognized that the carbonation resistance of cementitious materials depends on two main factors: one is CO_2 binding capacity and the other one is pore structure. In cement-based systems, portlandite and C − S−H gel phase (especially for blended cements where most portlandite has been consumed in pozzolanic reaction) are regarded as the main phases to be carbonated. However, the role of minor hydrates, e.g. hydrotalcite-like phase and monosulfate has been largely neglected, particularly when the slag substitution level is high, e.g. CEM III/B, or 70 wt.% in the present research, and alkali-activated slag systems. The authors believe that influence of slag chemistry on the CO_2 binding capacity of slag cement paste deserves a deeper discussion, in which the CO_2 binding ability of different phases should be emphasized (Here we defined the results measured from fully carbonated area (see Figure 7) as ***CO_2 binding capacity***. Six months of accelerated carbonation test was performed in the study, and we considered that the surface area had (nearly) been carbonated completely.). Data from this article and Table 3 in [28] (for slag M0, M8, and M16 with increasing MgO contents) would be analyzed together to cover the common range of slag chemistry.

Figure 14 demonstrates that the areas under MS CO_2 curves, or CO_2 binding capacity of the specimens increased significantly with the increasing MgO content from slag M0 to M16 blend; however, Al_2O_3 seemed to have negligible effect on CO_2 binding capacity. In other words, the enhanced ettringite and monosulfate formations with increasing alumina content in slag did not influence the CO_2 binding capacity positively. It was reasonable as the CO_2 concentration bound in carbonated Ca-Al AFm phases was stable, less than 1 wt.% (Table 3).

As shown in Tables 2 and 3, the absolute amount of CO_2 absorbed in each buffer phase increased when shifting from mildly carbonated to fully carbonated area. However, the proportions distributed among these buffer phases revealed an important finding (Figure 15). Irrespective of alumina content, the proportion of CO_2 absorbed into carbonated Ca-Al AFm phases plus

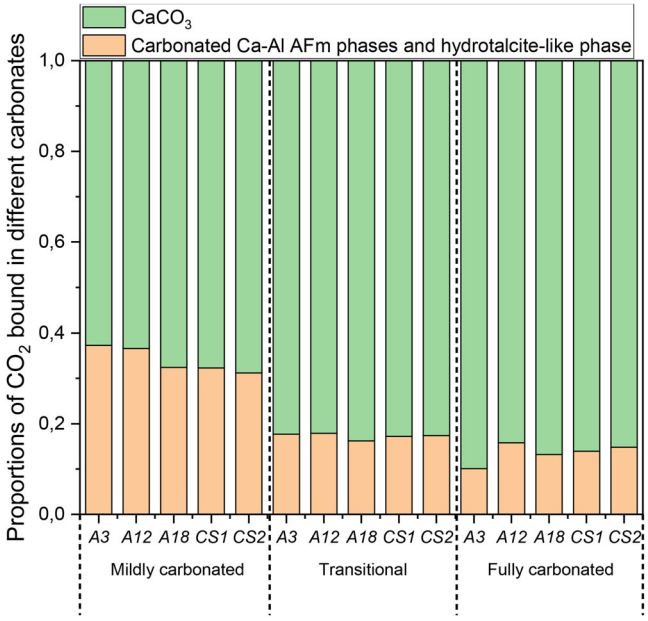

Figure 15. The proportions of CO_2 bound in $CaCO_3$ and carbonated Ca-Al AFm phases plus hydrotalcite-like phase from mildly to fully carbonated area of each mixture.

hydrotalcite-like phase decreased while that from calcium carbonate increased. It provided a deeper understanding of the carbonation behavior of slag-rich blends. Initially, monosulfate, hydrotalcite-like phase, portlandite, and C – S–H gel phase acted as the CO_2 binding phases together. Especially for monosulfate and hydrotalcite-like phase, they shared around 30% CO_2 in the mildly carbonated area due to their stacked layer morphologies, and this value decreased to ~20% in the transitional area and less than 20% in the fully carbonated area. It can be suggested that there is a limit for the stacked layer structure to absorb CO_2, when the space between layers is occupied by CO_2 completely, CO_2 can only be fixed into calcium carbonate (Portlandite and C – S–H gel phase in particular with large specific surface area reacted with CO_2 continuously.). Therefore, the proportion of CO_2 bound in calcium carbonate went up under continuous CO_2 attack. Note that contrary to the reaction between CO_2 and C – S–H gel phase which is a volume decrease reaction, the stacked layer structure can maintain its structure and would not lead to a pore structure coarsening during carbonation.

4.2. *Slag reactivity vs. carbonation resistance of cement-slag system*

Al_2O_3-rich slag cement paste shows good performance at the early age of hydration [13, 15]. Based on R3 and dissolution tests, our previous work verified that slag reactivity positively affected by its alumina content [17]. Besides, three levels of reactivity were classified, i.e. low reactivity (slag M0 and A3), medium reactivity (slag M8, A12, CS1, and CS2), and high reactivity (slag M16 and A18). However, when estimating the carbonation resistance of these cement-slag mixtures according to two important parameters, i.e. pore structure and CO_2 binding capacity [24], the classification employed for reactivity was not applicable anymore.

Yet, cement-slag M16 mixture exhibited the best carbonation resistance. It showed the least carbonation depth based on phenolphthalein spray (5–10 mm) (For the results regarding slag M0, M8, and M16, please refer to Figure 9 in [28].), the highest CO_2 binding capacity (Figure 14), and the smallest critical pore diameter after carbonation. As for slag M0, CS1, and CS2, they presented the worst carbonation resistance when blended with cement. Their carbonation depths were much greater (close to 20 mm), and they displayed a bimodal pore structure with larger pore volume after carbonation. For slag M8, A3, A12, and A18, they showed a medium carbonation resistance in the slag rich cement pastes with similar CO_2 binding capacity.

Although high alumina content slag cement pastes (CS1 (14.51 wt.%), CS2 (17.12 wt.%), and A18 (18.19 wt.%)) show good early age performance due to the enhanced formation of ettringite and monosulfate, they do not perform equally good against CO_2 attack. The specimens with CS1 and CS2 formed a relatively larger critical pore diameter after 3 months of curing (10–20 nm as shown in Figure 10(a)), which was the main reason for their lower carbonation resistance compared to other specimens. In other words, the adverse effect of CaO/SiO_2 ratio reduction on the hydration can be compensated by higher amount of Al_2O_3 but the same argument cannot be extended to the carbonation resistance. For instance, the slag A18 paste showed a mediocre carbonation resistance. This behavior can be explained by taking the following two aspects into consideration. Firstly, enhanced monosulfate formations (due to high alumina content) do not influence the CO_2 binding capacity positively. Secondly, aluminum uptake in C – S–H gel phase increases the amount of bridging silicate tetrahedra [55], and a greater

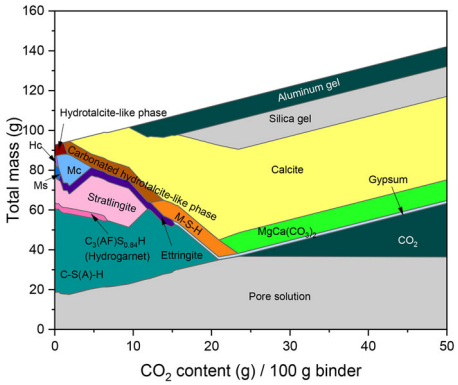

Figure 16. Thermodynamic modeling of the phase assemblages in A18 paste during the step-wise carbonation. Hc: calcium hemicarbonate; Mc: calcium monocarbonate; Ms: calcium monosulfoaluminate.

number of polymerized units commonly exhibit a better carbonation resistance by the limited CO_2 access [57, 58]. Thus, the CO_2 binding capacity seemed to be unaffected by the Al_2O_3 content in slag (Figure 14).

4.3. *Thermodynamic modeling*

Figure 16 illustrates the thermodynamic modeling results of phase assemblage evolution during the stepwise carbonation, using cement-slag A18 paste as an example. The reaction degree of clinker phases of cement at 90 days was estimated using the empirical kinetic approach of Parrot and Killoh [59], and the parameters were reported by Lothenbach et al. in [60]. The hydration degree of slag A18 was estimated to be 30% after 3 months of curing. For simplicity, it was assumed that slag dissolved congruently.

At zero CO_2 addition, $C-S(A)-H$ gel phase was modeled as the main hydration product. Hydrotalcite-like phase, monosulfate, hydrogarnet, and strätlingite was also predicted to be formed, which were identified in slag-rich cement paste systems by other researchers [61, 62]. With the gradual addition of CO_2 into the system, the change in phase assemblage started to occur. For the decalcification of $C-S(A)-H$ gel phase, readers can refer to [63]. Calcite was predicted to be the only form of $CaCO_3$, although different morphologies of $CaCO_3$ were detected in real samples [32, 43, 44] and in this study. The focus of this modeling study was the phase transition of Al-bearing and SO_4-bearing phases after CO_2 addition.

After the decomposition of monosulfate, ettringite was modeled to be the main sulfate-bearing phase (intermediate), which was further carbonated to yield gypsum. However, no gypsum was detected in the present study and other blended cement systems [20, 24]. Probably this secondary gypsum was amorphous [64], or the amount of sulfate in the system was too low as it was formed in the carbonated super-sulfated cement paste [65]. Besides, sulfate ions can also be absorbed by amorphous silica gel formed after carbonation. This factor should be considered in further study. As for the transformation routine of Al-bearing phases, monosulfate and strätlingite started to decompose upon CO_2 contact. Hemi- and monocarbonates were predicted as intermediates. Monocarbonate was decomposed into calcite and subsequently to strätlingite as the carbonation proceeded. Hydrogarnet persisted initially and transformed into strätlingite with the continuous CO_2 attack. Al-gel was predicted as the final Al-bearing phase. Apparently, several disagreements existed between GEMS modeling and experimental results. It should be noted that the formation of hemi- and mono-carbonates was not observed by XRD or TGA in this study at any carbonation depth. The authors considered that monosulfate (including other Ca-Al AFm phases) would not decompose during carbonation and absorb CO_2 into interlayer space because of its layered microstructure. It was consistent with the results in [47], which also concluded that monosulfate can incorporate some carbonates, forming carbonate/sulfate-AFm solid solution.

5. Conclusions

This study investigated the carbonation characteristics of predefined cement-slag systems through accelerated carbonation test, and attempted to build a connection among slag chemistry, slag reactivity, and carbonation resistance of the system. The main conclusions drawn were as follows:

- After accelerated carbonation testing, three CO_2 binding phases were identified irrespective of the gradual addition of alumina content in slag, i.e. carbonated Ca-Al AFm phases (amorphous or nano-crystalline), carbonated hydrotalcite-like phase, and calcium carbonate (vaterite and calcite).
- The critical pore diameter of slag cement pastes increased to the range of 0.1–10 μm after carbonation. A bimodal pore structure and significantly larger pore volume appeared in the carbonated CS1 and CS2 slag pastes.
- Carbonated Ca-Al AFm phases and hydrotalcite-like phase bound around 30% of the total CO_2 that diffused into the mildly carbonated area. This value decreased to about 20% in the transitional area and less than 20% in the fully carbonated area.
- The CO_2 binding capacity of each mixture was similar, fluctuating at 15–20 wt.% in the completely carbonated area. In other words, the enhanced ettringite and calcium monosulfoaluminate formation with the increasing alumina content did not exert a positive influence on CO_2 binding capacity.
- The slag reactivity classification method [17] proposed earlier by the authors cannot be extended to predict carbonation resistance of a cement-slag system directly. The main challenge occurred for slags with high alumina content. Our experiments showed that Al_2O_3-rich slag

was reactive as a blended cement component, but it did not contribute to carbonation resistance.

Note that the investigations carried out in this paper and [28] were mainly based on synthetic slags, and more research should be performed in the future to confirm the applicability of these conclusions for commercial slags. Furthermore, it was noticed that there was a trend for consistent production of lime-rich slag in steelmaking manufacturing [66]. However, for synthetic slags considered in our research, the CaO/SiO_2 ratio was kept at around 1. It deserves further research that whether this continuous increasing in CaO content in slag (i.e. $CaO/SiO_2 \gg 1$) can enhance the performance of blended cement paste.

Acknowledgments

Authors also thank Arjan Thijssen (Microlab, Delft University of Technology) for his technical help.

Disclosure statement

No potential conflict of interest was reported by the authors.

Funding

The authors are grateful for the China Scholarship Council (Grant Number 201808320456) and BAM Infraconsult B.V. for their financial support.

References

[1] Yang Y, Raipala K, Holappa L. Ironmaking. In: Treatise on process metallurgy. Amsterdam: Elsevier; 2014.
[2] Sohn I, Min DJ. A review of the relationship between viscosity and the structure of calcium-silicate-based slags in ironmaking. Steel Research Int. 2012;83(7): 611–630. doi:10.1002/srin.201200040.
[3] Juenger MC, Snellings R, Bernal SA. Supplementary cementitious materials: new sources, characterization, and performance insights. Cem Concr Res. 2019;122: 257–273. doi:10.1016/j.cemconres.2019.05.008.
[4] Piatak NM, Parsons MB, Seal RR. II, Characteristics and environmental aspects of slag: a review. Appl Geochem. 2015;57:236–266. doi:10.1016/j.apgeochem.2014.04.009.
[5] De Belie N. Properties of fresh and hardened concrete containing supplementary cementitious materials. Vol. 25. Berlin: Springer; 2018.
[6] Özbay E, Erdemir M, Durmuş Hİ, et al. Utilization and efficiency of ground granulated blast furnace slag on concrete properties – a review. Constr Build Mater. 2016;105:423–434. doi:10.1016/j.conbuildmat.2015.12.153.
[7] Lothenbach B, Scrivener K, Hooton R. Supplementary cementitious materials. Cem Concr Res. 2011;41(12): 1244–1256. doi:10.1016/j.cemconres.2010.12.001.
[8] Pietersen HS. Reactivity of fly ash and slag in cement. Delft: TU Delft; 1993.
[9] Escalante JI, Gómez LY, Johal KK, et al. Reactivity of blast-furnace slag in Portland cement blends hydrated under different conditions. Cem Concr Res. 2001;31(10): 1403–1409. doi:10.1016/S0008-8846(01)00587-7.
[10] Bougara A, Lynsdale C, Milestone NB. Reactivity and performance of blastfurnace slags of differing origin. Cem Concr Compos. 2010;32(4):319–324. doi:10.1016/j.cemconcomp.2009.12.002.
[11] Schöler A, Winnefeld F, Haha MB, et al. The effect of glass composition on the reactivity of synthetic glasses. J Am Ceram Soc. 2017;100(6):2553–2567. doi:10.1111/jace.14759.
[12] Kucharczyk S, Zajac M, Stabler C, et al. Structure and reactivity of synthetic CaO-Al2O3-SiO2 glasses. Cem Concr Res. 2019;120:77–91. doi:10.1016/j.cemconres.2019.03.004.
[13] Blotevogel S, Ehrenberg A, Steger L, et al. Ability of the R3 test to evaluate differences in early age reactivity of 16 industrial ground granulated blast furnace slags (GGBS). Cem Concr Res. 2020;130:105998. doi:10.1016/j.cemconres.2020.105998.
[14] Blotevogel S, Steger L, Hart D, et al. Effect of TiO2 and 11 minor elements on the reactivity of ground-granulated blast-furnace slag in blended cements. J Am Ceram Soc. 2021;104(1):128–139. doi:10.1111/jace.17431.
[15] Whittaker M, Zajac M, Ben Haha M, et al. The role of the alumina content of slag, plus the presence of additional sulfate on the hydration and microstructure of Portland cement-slag blends. Cem Concr Res. 2014;66: 91–101. doi:10.1016/j.cemconres.2014.07.018.
[16] Snellings R, Li X, Avet F, et al. Rapid, robust, and relevant (R3) reactivity test for supplementary cementitious materials. Aci Mater J. 2019;116(4):155–162. doi:10.14359/51716719.
[17] Zhang Y, Zhang S, Chen Y, et al. The effect of slag chemistry on the reactivity of synthetic and commercial slags. Constr Build Mater. 2022;335:127493. doi:10.1016/j.conbuildmat.2022.127493.
[18] Papadakis VG. Effect of supplementary cementing materials on concrete resistance against carbonation and chloride ingress. Cem Concr Res. 2000;30(2):291–299. doi:10.1016/S0008-8846(99)00249-5.
[19] Sulapha P, Wong SF, Wee TH, et al. Carbonation of concrete containing mineral admixtures. J Mater Civ Eng. 2003;15(2):134–143. doi:10.1061/(ASCE)0899-1561(2003)15:2(134).
[20] Borges PH, Costa JO, Milestone NB, et al. Carbonation of CH and C–S–H in composite cement pastes containing high amounts of BFS. Cem Concr Res. 2010;40(2): 284–292. doi:10.1016/j.cemconres.2009.10.020.
[21] Bucher R, Diederich P, Escadeillas G, et al. Service life of metakaolin-based concrete exposed to carbonation: comparison with blended cement containing fly ash, blast furnace slag and limestone filler. Cem Concr Res. 2017;99:18–29. doi:10.1016/j.cemconres.2017.04.013.
[22] Shah V, Bishnoi S. Carbonation resistance of cements containing supplementary cementitious materials and its relation to various parameters of concrete. Constr Build Mater. 2018;178:219–232. doi:10.1016/j.conbuildmat.2018.05.162.
[23] Wu B, Ye G. Development of porosity of cement paste blended with supplementary cementitious materials after carbonation. Constr Build Mater. 2017;145:52–61. doi:10.1016/j.conbuildmat.2017.03.176.
[24] von Greve-Dierfeld S, Lothenbach B, Vollpracht A, et al. Understanding the carbonation of concrete with supplementary cementitious materials: a critical review by RILEM TC 281-CCC. Mater Struct. 2020;53(6): 1–34. doi:10.1617/s11527-020-01558-w.
[25] Sevelsted TF, Skibsted J. Carbonation of C–S–H and C–a–S–H samples studied by 13C, 27Al and 29Si MAS NMR spectroscopy. Cem Concr Res. 2015;71:56–65. doi:10.1016/j.cemconres.2015.01.019.
[26] Wu B, Ye G. Carbonation mechanism of different kind of CSH: rate and products. In: International RILEM

conference on materials, systems and structures in civil engineering 2016-Segment on concrete with supplementary cementitious materials. 22–24 August 2016; Lyngby, Denmark. Rilem PRO 113; 2016, p. 163–272.
[27] Liu X, Feng P, Cai Y, et al. Carbonation behaviors of calcium silicate hydrate (CSH): effects of aluminum. Constr Build Mater. 2022;325:126825. doi:10.1016/j.conbuildmat.2022.126825.
[28] Zhang Y, Liang M, Gan Y, et al. Effect of MgO content on the quantitative role of hydrotalcite-like phase in a cement-slag system during carbonation. Cem Concr Compos. 2022;134:104765. doi:10.1016/j.cemconcomp.2022.104765.
[29] Zunino F, Scrivener K. Factors influencing the sulfate balance in pure phase C3S/C3A systems. Cem Concr Res. 2020;133:106085. doi:10.1016/j.cemconres.2020.106085.
[30] Antoni M, Rossen J, Martirena F, et al. Cement substitution by a combination of metakaolin and limestone. Cem Concr Res. 2012;42(12):1579–1589. doi:10.1016/j.cemconres.2012.09.006.
[31] Zhang Y, Wan Z, de Lima Junior LM, et al. Early age hydration of model slag cement: interaction among C3S, gypsum and slag with different Al2O3 contents. Cem Concr Res. 2022;161:106954. doi:10.1016/j.cemconres.2022.106954.
[32] Thiery M, Villain G, Dangla P, et al. Investigation of the carbonation front shape on cementitious materials: effects of the chemical kinetics. Cem Concr Res. 2007;37(7):1047–1058. doi:10.1016/j.cemconres.2007.04.002.
[33] Wagner T, Kulik DA, Hingerl FF, et al. GEM-Selektor geochemical modeling package: TSolMod library and data interface for multicomponent phase models. Canadian Mineralogist. 2012;50(5):1173–1195. doi:10.3749/canmin.50.5.1173.
[34] Kulik DA, Wagner T, Dmytrieva SV, et al. GEM-Selektor geochemical modeling package: revised algorithm and GEMS3K numerical kernel for coupled simulation codes. Comput Geosci. 2012;17(1): p):1–24. doi:10.1007/s10596-012-9310-6.
[35] Hummel W, et al. Nagra technical report NTB 02-16. Wettingen, Switzerland, 2002.
[36] Hummel W, Berner U, Curti E, et al. Nagra/PSI chemical thermodynamic data base 01/01. Radiochimica Acta. 2002;90(9-11):805–813. doi:10.1524/ract.2002.90.9-11_2002.805.
[37] Matschei T, Lothenbach B, Glasser FP, et al. Thermodynamic properties of Portland cement hydrates in the system CaO–Al2O3–SiO2–CaSO4–CaCO3–H2O. Cem Concr Res. 2007;37(10):1379–1410. doi:10.1016/j.cemconres.2007.06.002.
[38] Lothenbach B, Matschei T, Möschner G, et al. Thermodynamic modelling of the effect of temperature on the hydration and porosity of Portland cement. Cem Concr Res. 2008;38(1):1–18. doi:10.1016/j.cemconres.2007.08.017.
[39] Myers RJ, Bernal SA, Provis JL. A thermodynamic model for C-(N-) ASH gel: CNASH_ss. Derivation and validation. Cem Concr Res. 2014;66:27–47. doi:10.1016/j.cemconres.2014.07.005.
[40] Myers RJ, Lothenbach B, Bernal SA, et al. Thermodynamic modelling of alkali-activated slag cements. Appl Geochem. 2015;61:233–247. doi:10.1016/j.apgeochem.2015.06.006.
[41] Ke X, Bernal SA, Provis JL, et al. Thermodynamic modelling of phase evolution in alkali-activated slag cements exposed to carbon dioxide. Cem Concr Res. 2020;136:106158. doi:10.1016/j.cemconres.2020.106158.
[42] Miyata S. Anion-exchange properties of hydrotalcite-like compounds. Clays Clay Miner. 1983;31(4):305–311. doi:10.1346/CCMN.1983.0310409.
[43] Villain G, Thiery M, Platret G. Measurement methods of carbonation profiles in concrete: Thermogravimetry, chemical analysis and gammadensimetry. Cem Concr Res. 2007;37(8):1182–1192. doi:10.1016/j.cemconres.2007.04.015.
[44] Morandeau A, Thiery M, Dangla P. Investigation of the carbonation mechanism of CH and CSH in terms of kinetics, microstructure changes and moisture properties. Cem Concr Res. 2014;56:153–170. doi:10.1016/j.cemconres.2013.11.015.
[45] Herterich J, Richardson I, Moro F, et al. Microstructure and phase assemblage of low-clinker cements during the early stages of carbonation. Cem Concr Res. 2022;152:106643. doi:10.1016/j.cemconres.2021.106643.
[46] Zhang Y, Çopuroğlu O. The role of hydrotalcite-like phase and monosulfate in slag cement paste during atmospheric and accelerated carbonation. Cem Concr Compos. 2022;132:104642. doi:10.1016/j.cemconcomp.2022.104642.
[47] Georget F, Lothenbach B, Wilson W, et al. Stability of hemicarbonate under cement paste-like conditions. Cem Concr Res. 2022;153:106692. doi:10.1016/j.cemconres.2021.106692.
[48] Zajac M, Lechevallier A, Durdzinski P, et al. CO2 mineralisation of Portland cement: towards understanding the mechanisms of enforced carbonation. J CO2 Util. 2020;38:398–415. doi:10.1016/j.jcou.2020.02.015.
[49] Okada Y, et al. Relationship between NMR 29 Si chemical shifts and FT-IR wave numbers in calcium silicates. In: Nuclear magnetic resonance spectroscopy of cement-based materials. Berlin: Springer; 1998, p. 69–78.
[50] Black L, Breen C, Yarwood J, et al. Structural features of C–S–H (I) and its carbonation in air—a raman spectroscopic study. Part II: carbonated phases. J Am Ceramic Soc. 2007;90(3):908–917. doi:10.1111/j.1551-2916.2006.01429.x.
[51] Rimmelé G, Barlet-Gouédard V, Porcherie O, et al. Heterogeneous porosity distribution in Portland cement exposed to CO2-rich fluids. Cem Concr Res. 2008;38(8-9):1038–1048. doi:10.1016/j.cemconres.2008.03.022.
[52] Kloproggea JT, Kristófb J, Frosta RL. Thermogravimetric analysis-mass spectrometry (TGA-MS) of hydrotalcites containing CO32−, NO3−, Cl−, SO42− or ClO4−. Clay Odyssey. 2001;1:451.
[53] Ngala V, Page C. Effects of carbonation on pore structure and diffusional properties of hydrated cement pastes. Cem Concr Res. 1997;27(7):995–1007. doi:10.1016/S0008-8846(97)00102-6.
[54] Frías M, Goñi S. Accelerated carbonation effect on behaviour of ternary Portland cements. Compos Part B: Eng. 2013;48:122–128. doi:10.1016/j.compositesb.2012.12.008.
[55] Richardson I. Tobermorite/jennite-and tobermorite/calcium hydroxide-based models for the structure of CSH: applicability to hardened pastes of tricalcium silicate, β-dicalcium silicate, Portland cement, and blends of Portland cement with blast-furnace slag, metakaolin, or silica fume. Cem Concr Res. 2004;34(9):1733–1777. doi:10.1016/j.cemconres.2004.05.034.
[56] Zajac M, Skibsted J, Durdzinski P, et al. Kinetics of enforced carbonation of cement paste. Cem Concr Res. 2020;131:106013. doi:10.1016/j.cemconres.2020.106013.
[57] Li J, Yu Q, Huang H, et al. Effects of Ca/Si ratio, aluminum and magnesium on the carbonation behavior of calcium silicate hydrate. Materials. 2019;12(8):1268. doi:10.3390/ma12081268.
[58] Irbe L, et al. The role of aluminium in CASH during chemical attack on concrete. In: Second International

Conference on the Chemistry of Construction Materials-ICCCM 2016. 2016.
[59] Parrot L. Prediction of cement hydration in *Proceedings of the British Ceramic Society*. 1984.
[60] Lothenbach B, Le Saout G, Gallucci E, et al. Influence of limestone on the hydration of Portland cements. Cem Concr Res. 2008;38(6):848–860. doi:10.1016/j.cemconres.2008.01.002.
[61] Taylor HF. Cement chemistry. Vol. 2. London: Thomas Telford; 1997.
[62] Luke K, Lachowski E. Internal composition of 20-year-old fly ash and slag-blended ordinary Portland cement pastes. J Am Ceramic Soc. 2008;91(12):4084–4092. doi:10.1111/j.1551-2916.2008.02783.x.
[63] Shi Z, Lothenbach B, Geiker MR, et al. Experimental studies and thermodynamic modeling of the carbonation of Portland cement, metakaolin and limestone mortars. Cem Concr Res. 2016;88:60–72. doi:10.1016/j.cemconres.2016.06.006.
[64] Justnes H, Skocek J, Østnor TA, et al. Microstructural changes of hydrated cement blended with fly ash upon carbonation. Cem Concr Res. 2020;137:106192. doi:10.1016/j.cemconres.2020.106192.
[65] Xie Y, Sun T, Shui Z, et al. The impact of carbonation at different CO2 concentrations on the microstructure of phosphogypsum-based supersulfated cement paste. Constr Build Mater. 2022;340:127823. doi:10.1016/j.conbuildmat.2022.127823.
[66] Zhang Y, Saravanakumar K, Çopuroğlu O. EDS micro-analysis of unhydrated blast furnace slag grains in field concrete with different service life. Microsc Microanal. 2022;28(5):1–11. doi:10.1017/S1431927622000848.